INTERACTIONS OF FLUID OXYGEN DROPS IN FLUID HYDROGEN AT ROCKET CHAMBER PRESSURES

K. Harstad and J. Bellan
Jet Propulsion Laboratory
California Institute of Technology
Pasadena, CA. 91109

Abstract

A model of fluid drop behavior in clusters has been developed including the interactions induced by the drop proximity. The model is based upon the global conservation equations for the cluster coupled to isolated fluid drop equations previously developed. Heat and mass transfer to the cluster are modeled using the Nusselt number concept. Results from calculations for the $LO_x - H_2$ system show the predictions to be insensitive to the value of the Nusselt number over three orders of magnitude. The results also show that at fixed pressure, increased drop proximity induces increased accumulation of LO_x in the interstitial space inside the cluster. At fixed initial drop proximity, the gradients of the dependent variables become increasingly smeared as the pressure increases; an opposite result from that obtained for isolated drops. It is thus inferred that clusters of drops might be a desirable aspect in supercritical combustion because they aid mixing of the reactive components.

1. Introduction

In liquid rocket motors atomization of the liquid oxygen occurs either by means of coaxial jets of LO_x surrounded by a hydrogen stream, or by means of impinging jets (either $LO_x - LO_x$, or $LO_x - fuel$ which promotes mixing of reactants). Experimental observations of atomization of coaxial jets by Hardalupas et al. [1] and Engelbert et al. [2] reveals the initial formation of ligaments, each ligament quickly disintegrating into a cluster of drops. Similarly, visualizations of impinging liquid jets [3] have shown that under both cold and hot flow conditions the jets breakup in a periodic manner into ligaments which further break up into drops thereby creating clusters of drops. Recent observations by Ryan et al. [4] have documented this typical breakup process while also yielding information regarding the breakup length and the drop size for both laminar and turbulent, impinging jets. Poulikakos [5] made similar observations.

These observations indicate that fluid drops created during atomization in liquid rocket chambers do not behave as isolated and instead have a collective behavior. This realization is very important for controlling high frequency combustion instabilities because the response function must incorporate this fluid drop interaction.

Fluid drop interaction at high pressure has been modeled by Jiang and Chiang [6] using the concept of 'sphere of influence' of Bellan and Cuffel [7] and results were obtained for n-pentane

adiabatic drop arrays where the drops are uniformly distributed ancl stationary. The model of Jiang and Chiang [6] does not include the intricacies of high pressure transport processes ancl thus it is not appropriate for the supercritical regime where Fick's and Fourier's laws are no longer solely valid to completely describe the transport, matrix [8]. Additionally, the interdrop distance does not have similar values under subcritical and supercritical conditions since in the former situation the liquid drops have a motion distinct from that of the surrounding gas whereas in the latter situation, because the densities of the two fluids are more similar, their motion is more similar as well. Moreover, the dense spray effects identified at subcritical conditions were the consequence of both high mass and high volume loading; in supercritical conditions, the high volume loading is not necessarily accompanied by high mass loading because of the density ratio effect. This means that dense spray effects will be encountered in supercritical conditions only for interdrop distances much smaller than in subcritical conditions. In fact, dense spray effects will visually manifest as small scale density variations, consistent with the discussed observations for coaxial and impinging jets atomization [1], [2], [4] and [5].

This study is based upon the isolated fluid drop model developed by Harstad and Bellan [8] and genuinely takes into account fluid drop interaction because the drops are not stationary with respect to each other, but move as a consequence of the $LO_x - H_2$ interdiffusion which changes the radius of the sphere of influence. Thus, the equations developed in [8] for isolated drops are used here with boundary conditions calculated using the global cluster model developed below; in Harstad and Bellan [8] the boundary conditions were prescribed to be those of the surrounding fluid.

2. Model

The configuration studied is that of a general-volume-shape cluster of N monodisperse fluid drops immersed into a dense gas. The interstitial region between drops is uniform and quiescent with respect to the cluster; the implication is that while turbulence is strong enough to mix the interstitial region, it does not affect the regions near the drops. By definition, the 'sphere of influence' around each drop is centered at the drop center and has a radius, R_{si}, whose value is half of the distance between adjacent drops. The volume of the sphere of influence, V_{si}, contains the drop and its surrounding fluid, and has a fixed mass; this means that the V_{si} boundary is a function of time to accommodate the change in density due to heating. The volume of the interstitial region of the cluster is

$$Vi = V_C - NV_{si} \tag{2.1}$$

and it is in this volume that the conservation equations arc stated below in a Lagrangian frame.

- conservation of mass

$$\frac{dp}{dt} = 0 \tag{2.2}$$

- conservation of species j

$$\frac{d\rho_j}{dt} = -m_j \nabla \cdot \vec{J}_j \tag{2.3}$$

- conservation of energy

$$\frac{d(\rho e)}{dt} = -\nabla \cdot \vec{q} \tag{2.4}$$

where e = $h/m - p/p$.

To obtain the coupling among all fluid chops, we integrate over V_i and S_i

$$\frac{d}{dt}(\int_{V_i} \rho dV) = 0 \tag{2.5}$$

$$\frac{d}{dt}(\int_{V_i} \rho_j dV) = -\int_{S_i} m_j \vec{J}_j \cdot d\vec{A}_{S_i} \tag{2.6}$$

$$\frac{d}{dt}[\int_{V_i} (\rho h/m - p) dV] = -\int_{S_i} \vec{q} \cdot d\vec{A}_{S_i} \tag{2.7}$$

accounting for the null relative velocity with respect to S_i.

Equation 2.5 has a simple integral

$$V_i(t) = M_i/\rho_i \tag{2.8}$$

The species and heat contributions to *Vi* arise both from the interaction of the cluster with its surroundings through fluxes of species and heat across S_i, and from the interaction of V_i with all drops. Thus, Eqs.2.6 and 2.7 can be rewritten

$$\sim \quad = \quad \frac{m_j}{M_{.l}}(J_{je}A_C - NJ_{j,si}A_{si}) \tag{2.9}$$

$$\frac{d}{dt}(h_i/m_i - p_e/\rho_i) = \frac{1}{M_i}(q_e A_C - Nq_{si}A_{si}) \tag{2.10}$$

Using thermodynamic relationships, for a two component system, Eq. 2.10 can be transformed into an equation for T_i

$$\tilde{C}_V \frac{dT_i}{dt} = \frac{1}{M_i}[(q_e - m_1\tilde{h}_i J_{1e})A_C - N(q_{si} - m_1\tilde{h}_i J_{1,si})A_{si}] - \tilde{\kappa}_s \frac{p_e}{\rho_i}\frac{dp_e}{dt} \tag{2.11}$$

where

$$\tilde{C}_V \equiv C_p/m - \alpha_v \frac{p}{\rho}, \tilde{\kappa}_s \equiv \kappa_s - \tilde{C}_V \frac{m\alpha_v T}{p\tilde{C}_p}, \tilde{h} \equiv (\frac{h_1}{m_1} - \frac{h_2}{m_2}) - p(\frac{v_1}{m_1} - \frac{v_2}{m_2})$$

The values of $J_{1,si}$ and q_{si} are calculated at the edge of the sphere of influence according to the model of Harstad and Bellan [8].

To calculate J_{1e} and q_e, *we* recall the formalism introduced in [8] where the fluxes were calculated from a transport matrix according to the fluctuation theory of Keizer [9]. In this formalism, the fluxes are linear combinations of the temperature, pressure and mass fraction gradients where the multiplying factors for each term are calculated from transport properties and thermodynamic data such as equations of state. Since in the present study it is only the temperature ancl the mass fractions that vary in the cluster surroundings, for a binary composition $(LO_x - H_2)$

$$J_{1e} = A_J^{(i)}\frac{\partial Y_1}{\partial x} + B_J^{(i)}\frac{\partial T}{\partial x}, \; q_e = A_q^{(i)}\frac{\partial T}{\partial x} + C_q^{(i)}\frac{\partial Y_1}{\partial x} \tag{2.12}$$

where ; = 1 refers to LO_x, x is the direction normal to the. cluster surface enclosed by V_i and

$$A_J = \frac{mnD_m\alpha_D}{m_1}, \; B_J = \frac{m_2 nD_m(X_1X_2\alpha_T - m)}{mT} \tag{2.13}$$

$$A_q = \lambda - k_m \triangle h, C_q = \frac{m^2}{m_1 m_2}k_m T\alpha_D \tag{2.14}$$

$$k_m \equiv \alpha_T R_u nD_m, \; \overline{\triangle h} = \frac{m_1 m_2 X_1 X_2}{mR_u T}\left(\frac{h_1}{m_1} - \frac{h_2}{m_2}\right) \tag{2.15}$$

So far, the formulation is valid for any volume shape. Continuation of the model requires however the choice of a cluster volume shape; since the spherical shape is the simplest in this context, all further results will be valid for this particular case with the understanding that they could be generalized.

For a spherical cluster, the gradients can be approximated by a difference across an external length scale r_e as follows

$$\frac{\partial Y_1}{\partial r} = \frac{Y_{1e} - Y_{1i}}{r_e}, \; \frac{\partial T}{\partial r} = \frac{T_e - T_i}{r_e} \tag{2.16}$$

where r_e is related to what is equivalent to a Nusselt number and to the cluster radius through

$$r_e = R_C/Nu_C \tag{2.17}$$

since it is the characteristic distance over which transport occurs at the cluster surface. For a nonspherical cluster, an appropriate expression of Nu_C and a dimension equivalent to R_C (for example, $R_C = [3V_C/(4\pi)]^{1/3}$) could be used to define r_e.

Replacing Eqs. 2.13-2.17 **into** Eq. **2.12 yields**

$$(q_e - m_1\tilde{h}_i J_{1e})A_C = [3V_C/(4\pi)]^{1/3}4\pi Nu_C[(A_q^{(i)} - m_1\tilde{h}_i B_J^{(i)})(T_e - T_i) + (C_q^{(i)} - m_1\tilde{h}_i A_J^{(i)})(Y_{1e} - Y_{1i})] \tag{2.18}$$

$$J_{1e}A_C = [3V_C/(4\pi)]^{1/3}4\pi Nu_C[A_J^{(i)}(Y_{1e} - Y_{1i}) + B_J^{(i)}(T_e - T_i)] \tag{2.19}$$

which provides the necessary information for Eqs. 2.9 and 2.11. In this formulation, Nu_c *is a* parameter whose value is prescribed.

3. Solution procedure

The solution of the drop in its sphere of influence is discussed in detail in Harstad and Bellan [8]. In the interstitial region, the uuknowns are T_i aud Y_{1i} since pi is determined by the state equation. Once ρ_i is known, V_i and V_c are calculated. During each time step, the total differential equations 2.9 and 2.11 are solved using a second order predictor-corrector method in the manner described in [8].

4. Results

As discussed above, due to the essentially diffusive behavior at high pressure it is expected that dense spray effects will be important only for fluid-drops in closer proximity than in subcritical conditions. An experimentally verified [10] classification of various subcritical spray regimes according to the magnitude of the ratio R_{si}/R_d, identified the very dense regime as that corresponding to $R_{si}/R_d \leq 10$ [11]. Calculations with the above model were performed with a relatively large value of Nut, $Nu_C = 100$, in order to simulate the enhanced heat transfer for fluids at super critical conditions [12]. The results obtained with $R_d^0 = 50 \times 10^{-4}$ cm, $R_{si}^0 = 8R_d^0, R_C^0 = 2$ cm, $T_{db}^0 = 100$ K (T_d^0 is uniform inside the drop), $T_{si}^0 = T_e = 1000$ K, $p_e = 20$ MPa and Y_{1e} = O were essentially identical to those of the isolated drop exposed to surroundings at the external cluster conditions [8]. This finding indicates that under the conditions of this study, dense spray effects will be encountered at much smaller values of R_{si}/R_d.

The results presented below parallel that of Harstad and Bellan [8] for isolated drops. First, a baseline behavior is identified for dense spray effects and compared with the findings of [8] for external cluster conditions identical to the surrounding conditions of the isolated drop. Then, a parametric study follows paralleling that of [8] and the parametric variations found here are compared to those found in that study.

4.1, Baseline behavior and effect of the initial radius of the sphere of influence

The typical situation considered is: $R_d^0 = 50 \times 10^{-4}$ cm, $R_{si}^0 = 2R_d^0, R_C^0 = 2$ cm, $Nu_c = 100$, $T_{db}^0 = 100$ K (T_d^0 is uniform inside the drop), $T_{si}^0 = T^{\circ} = 1000$ K, $p_e = 20$ MPa and Y_{1e} = O. The number of drops in the cluster is 5.92×10^6.

Figure 1 illustrates the spatial profiles of T, Y_1 and ρ at different times while Fig. 2 depicts the time evolution of $T_{si}, Y_{1,si}, \rho_{si}, N_d, R_{si}$ and R_C. Comparisons between the calculated baseline results and those obtained for $R_{si}^0 = 5R_d^0$ and $R_{si}^0 = 10R_d^0$ (considered here typical of no drop interactions [8]) under otherwise identical conditions are presented in Fig. 3. While the baseline spatial variation of T, Y_1 and p parallels that obtained for the isolated drop in that it is mainly a cliff ision process, the closer drop proximity induces smaller density gradients (Fig. 3c), steeper Y_1 gradients (Fig. 3b) and larger temperatures as the initial interstitial temperature is equal to that of the cluster surroundings. An important difference among the results obtained with decreasing R_{si}^0/R_d^0 is the increased accumulation of a non-negligible amount of LO_x in the interstitial region (see Fig. 2a) as the cluster contracts due to heat being transferred faster from the interstitial region to the fluid LO_x drops than it is replenished from the cluster surroundings. This is consistent with the small decrease of T_{si}, R_{si} and R_C and the equivalent increase in ρ_{si} shown in Fig. 2. Eventually, T_{si} increases due to the increased amount of heat transferred to the cluster from its surroundings, and $Y_{1,si}$ accordingly decreases. All these effects are small for the values used in this baseline calculation; in particular, the value of Nu_c is too small for heat transfer from the cluster surroundings to replenish the heat relinquished by the interstitial fluid to the fluid drops. In fact, just as in subcritical cluster studies [11], the motion of the cluster boundary is governed by the ratio of two characteristic times: that of heat transferred from the interstitial region to the drops (a heat sink), t_1, and that transferred from the cluster surroundings to the cluster (a heat source), t_2; the only difference with the subcritical studies is the absence of phase change which requires a substantial heat budget. The latent, heat carried away by the evaporated compound in subcritical

situations constitutes a major percentage of the heat input to the gas phase. This explains the present, relatively undramatic cluster contraction and expansion.

The effect of drop proximity decreases with increasing pressure (Fig.3 and the more extensive study below), as the behavior becomes increasingly similar to pure diffusion. Additionally, the importance of chop interactions increases with increasing t_2 (decreasing Nu_C) since the heat transferred to the drops is replenished more slowly, and decreasing t_1 [(obtained by varying R_d^0 *(see* below) or by varying R_{si}^0/R_d^0 (see above)].

Elimination of the spatial variable between T and Y_1 (Fig.4) obtained in the baseline case shows that the solution is self-similar with respect to time away from the initial condition; a result difficult to predict *à priori.*

4.2. Effect of the cluster Nusselt number

As discussed above, the baseline value of Nu_C = *102* corresponds to $t_2 \gg t_1$. To study true competition between these two characteristic times, t_2 was decreased by increasing Nu_c to respectively 10^3, 10^4 and 10^5. The results illustrated in Fig. 5 show a surprisingly weak influence of Nu_C over a variation spanning three orders of magnitude. In agreement with the physics, with increased Nu_c the heat flux to the cluster increases and results in larger T_{si}, increased cluster expension and therefore smaller $Y_{1,si}$ and ρ_{si}.

The modeling of heat transfer to the cluster through the Nu_c **is** somewhat uncertain under supercritical conditions since the approach assumes the same length scale for T and Y_1. This assumption becomes increasingly questionable with increasing pressure and lack of experimental data precludes any definitive model.

4.3. Effect of the initial cluster radius

Since heat transfer to the cluster increases with the ratio S_C/V_C and thus with decreasing R_C^0, calculations were performed with baseline initial conditions except that now $R_C^0 = 1$ cm. Temporal plots (not presented) of $T_{si}, Y_{1,si}, \rho_{si}, N_d, R_{si}$ and R_c *show* that the results are virtually identical to those obtained with the larger cluster. Consistent with the weak Nu_c effect, the decrease in the number of drops in the cluster by a factor of 8 is inconsequential since the drop behavior is not governed by heat transfer to the cluster.

4.4. Effect of the initial fluid drop radius

The previous changes in the values of Nu_c and R_C^0 resulted in the variation of t_2; however, the ratio t_1/t_2 can also be changed by manipulating t_1. This is accomplished here by increasing R_d^0 to 100 x 10^{-4} cm. Since $R_{si}^0 = 2R_d^0$ and the cluster surface is the outer envelope of all spheres of influence, the number of drops decreases to 7.4 x 10^5.

Comparisons between the results obtained with larger drops and the baseline results appear in Fig. 6 for three different pressures. The larger drops heat up more slowly, maintain steeper density gradients for extended times and exhibit a larger variation in Y_1 with increasing pressure. In fact, plots of the interstitial values of $T_{si}, Y_{1,si}$ and ρ_{si} show that the same values are reached, but at larger times; thus, the effect of larger drops is that of a change in the characteristic time of the diffusion process that dominates at supercritical conditions.

4.5. Effect of the surrounding pressure

1'0 investigate the impact of chop interactions with surrounding pressure, extensive calculations were performed by changing p_e by almost an order of magnitude from 10 MPa to 80 MPa. The results are depicted in Fig. 7.

Unlike in the isolated drop situation [8] where gradients were greater with increasing pressure, here it is exactly the opposite. The effect of the drop interaction is to smear the gradients by increasing the cluster volume with increasing pressure. Although near the cluster boundary *Le* stays approximately constant with increasing pressure, Le_{eff} increases with pressure [13] indicating that heat diffusion increases with respect to mass diffusion. It is this relative increase in heat diffusion that promotes heat transfer to the cluster which results in increasing cluster expansion. In turn, this expansion causes an increase in the length scales and thus a smearing of the gradients. Thus, the presence of clusters of drops in burning sprays tends to render the dependent variables more uniform with increasing pressure whereas the opposite is true for isolated drops. In this respect, clusters of drops are a desirable aspect because they aid the mixing of the reactive components.

5. Summary and conclusions

A model of fluid drop behavior in clusters has been developed based upon a previous formulation for an isolated fluid drop. Transfer of heat and mass to the cluster from its surroundings has been modeled using a Nusselt number approach. Results obtained by varying the Nusselt number over 3 orders of magnitude show that the cluster behavior is not sensitive to the value of the Nusselt number. Consistent with this finding, the size of the cluster is also found to be a very weak parameter.

Since atomization of LO_x sprays into small fluid drops is considered desirable to design engineers, we have also studied the impact of the fluid drop size on the mass fraction distribution within the cluster. Larger fluid drops have a larger characteristic time and evolve similarly to the smaller drops except that the evolution time is proportionally stretched. Our results, therefore, agree with the well-known design practice of trying to atomize the LO_x jet into the smallest possible size fluid drops.

Parametric studies performed for the $LO_x - H_2$ system for various drop proximities show that the most important cluster effect is the accumulation of a non-negligible amount of LO_x with decreasing drop interdistance. The effect of drop proximity decreases with increasing pressure in that the behavior of the fluid drops in a very dense gas becomes increasingly similar to a pure diffusion process. For given initial drop proximity, an increase in pressure results in increased smearing of the gradients, a desirable aspect because it promotes mixing. This result, is exactly the opposite of what is obtained for isolated fluid drops [8].

ACKNOWLEDGMENT

This research was conducted at the Jet Propulsion Laboratory under sponsorship from the National Aeronautics and Space Administration, the George C. Marshall Space Flight, Center with Mr. Klaus W. Gross as technical contract monitor. His continuing interest and support, are greatly appreciated.

References

[1] Hardalupas, Y. Liu, C-H., Tsai, R-F. and White law, J. H., Coaxial atomization and combustion, *Proc. I UTA M Symp. on Mechanics and Combustion of Droplets and Sprays,* Tainan, Taiwan, R. O. C., 41-73 (1994)

[2] Engelbert, C. Hardalupas, Y. and Whitelaw, J. H., Breakup phenomena in coaxial airblast atomizers, *Proc. R. Sot. Lend., 451, 189-229 (1995)*

[3] Harrje, D. T. and Reardon, F. H., *Liquid Propellant Rocket Combustion Instability,* NASA SP-194 (1972)

[4] Ryan, H. M., Anderson, W. E., Pal, S. and Santoro, R. J., Atomization characteristics of impinging liquid jets, *J. Propulsion and Power,* **11(1), 135-145 (1995)**

[5] Poulikakos, **D., Determination of structure, temperature and concentration of the near injector region of impinging jets using holographic techniques,** *Proc. of the AFOSR Contractors Meeting, 275-278 (1993)*

[6] Jiang, T. L. and Chiang, W.-T., Effects of multiple drop interaction on droplet vaporization in subcritical and supercritical pressure environments, *Combust. and Flame, 97, 17-34 (1994)*

[7] Bellan, J. and Cuffel, R., A theory of non-dilute spray evaporation based upon multiple drop interaction, *Combust. and Flame,* 51(1), 55-67 (1983)

[8] Harstad, K. and Bellan, J., Isolated fluid oxygen drop behavior in fluid hydrogen at rocket chamber pressures, submitted (1997)

[9] Keizer, J., *Statistical Thermodynamics of Nonequilibrium Processes,* Springler-Verlag, New York, 1987

[10] Mizutani, Y., Nakabe, K., Fuchihata, M., Akamatsu, l?., Zaizen, M. and El-Emam, S. H., Spark-ignited spherical flames propagating in a suspended droplet cloud, *Atomization and Sprays, 3(2), 125-136 (1993)*

[11] Harstad, K. and Bellan, J., A model of the evaporation of binary-fuel cluster of drops, *Atomization and Sprays,* **1,** 367-388 (1991)

[12] Reid, R. C., Prausnitz, J. M. and Polling, B. E., *The Properties of Gases and Liquids,* 4th Edition, McGraw-Hill Book Company, 1987

[13] Harstad, K. and Bellan, J., The Lewis number under supercritical conditions, submitted (1997)

NOMENCLATURE

A	area of a surface
AJ, A_q	coefficients in the transport, matrix
B_J	coefficient in the transport matrix
C_p	molar heat capacity at constant pressure
C_q	coefficient in the transport matrix
D	diffusion coefficients
h	molar enthalpy
J	molar flux
Le	Lewis number
$Le_{,fj}$	effective Lewis number
m	molar mass
M	total mass
n	number of moles per unit volume
N	number of drops
N_d	drop number density in cluster
Nu_c	equivalent Nusselt number
p	pressure
q	heat flux
r	radial coordinate .
R_{si}	radius of the sphere of influence
R_d	drop radius
R_u	universal gas constant
S	surface
t	time
T	temperature
v	molar volume
V	volume
x	generic coordinate
X	mole fraction
Y	mass fraction

GREEK

α_D	mass cliff usion factors
α_T	thermal diffusion factor
α_v	thermal expansion ratio
κ_s	isentropic compressibility
λ	thermal conductivity
ρ	densit y

SUBSCRIPTS

b **boundary**
c at the cluster surface
d drop
e external to cluster
i interstitial
j species
m mass
si at the edge of the sphere of influence
T heat

SUPERSCRIPTS
i interstitial
O initial value

FIGURE CAPTIONS

Fig. 1 Spatial variation of the temperature (a), oxygen mass fraction (b) and density (c) at various times for R_d^0 = 50 x 10^{-4} cm, $R_{si}^0 = 2R_d^0$, R_C^0 = 2 cm, T_{db}^0 = 100 K , $Nu_C = 10^2$, $T_{si}^0 = T_e$ = **1000** K, p_e = 20 MPa and Y_{1e} = O. The curves correspond to the following times: 0.0 s (——), 2x1 0^{-3} s (- - -), 6x1 0^{-3} s (– · – o–), 8x1 0^{-3} s (· · · ·), 1.x1$0^{-2}$ S (— —), 1.08x10^{-2} S (– ··–).

Fig. 2 Time evolution of T_{si} and $Y_{1,si}$ (a), ρ_{si} and N_d (b), and R_{si} and R_C (c) for the same initial conditions as those in Fig. 1 caption.

Fig. 3 Spatial variation of the temperature (a), oxygen mass fraction (b) and density (c) at t = 10^{-2} s for $R_{si}^0 = 10R_d^0$ [p_e = 20 MPa (——), p_e = 80 MPa (· . ··)], $R_{si}^0 = 5R_d^0$ [p_e = 20 MPa (— –), p_e = 80 MPa (– ··–)] and $R_{si}^0 = 2R_d^0$ [p_e =20 MPa (- .- ·–), p_e =*80* MPa (· . ··)]. All other initial conditions are those of Fig. 1 caption.

Fig. 4 Oxygen mass fraction versus temperature for the initial conditions in the Fig. 1 caption.

Fig. 5 Time evolution of T_{si} and $Y_{1,si}$ (a), ρ_{si} and N_d (b), and R_{si} and R_C (c) for $Nu_C = 10^2$ (—); 10^3 (- - -); 10^4 (- .- .-); and 10^5 (· . ··). The other initial conditions are those of Fig. 1 caption.

Fig. 6 Spatial variation of the temperature (a), oxygen mass fraction (b) and density (c) at t = 10^{-2} s for R_d^0 = 50 x 10^{-4} cm [p_e =20 **MPa** (——), p_e = 40 MPa (- - -), p_e = 80 MPa (– . – .-)] and R_d^0 = **100 x 10^{-4} cm** [p_e = *20* MPa (· · · ·), p_e = 40 MPa (— —), p_e = 80 MPa (– . ·–)]. The other initial conditions are those of Fig. 1 caption.

Fig. 7 Spatial variation of the temperature (a), oxygen mass fraction (b) and density (c) at 1x 10^{-2} s for several pressures: 10 MPa (——), 15 MPa (- - -), 20 MPa (- . – ·–), 25 MPa (· . ··), 40 MPa (– –), 80 MPa (– . .–). Other initial conditions are those of Fig. 1 caption.

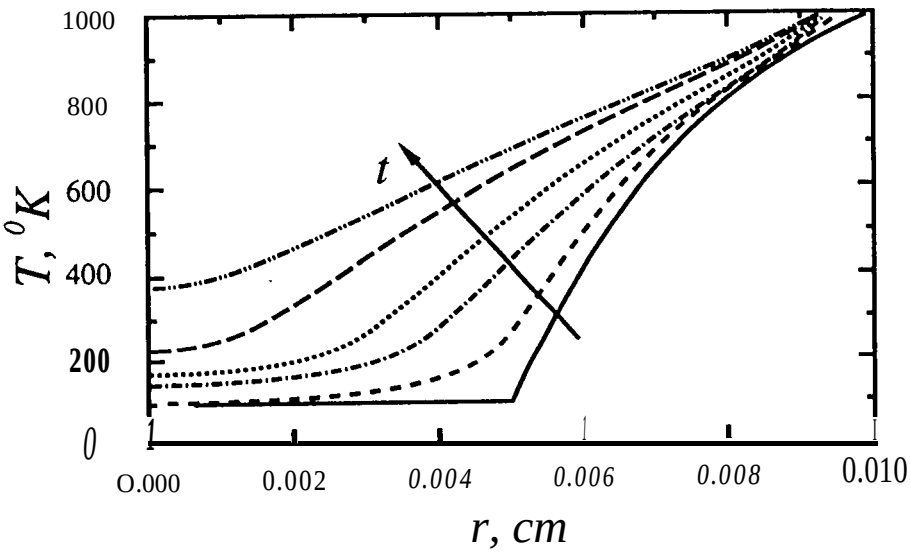

Fig 1a

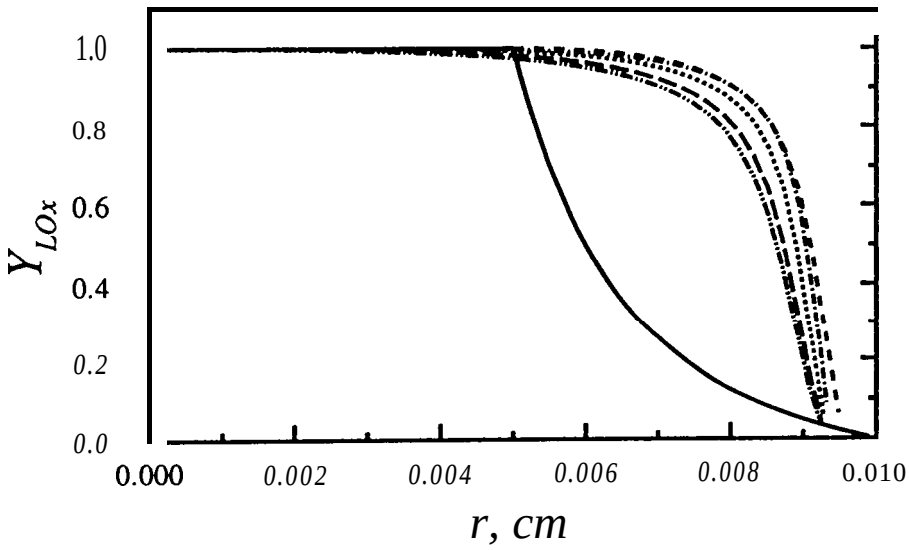

Fig 16

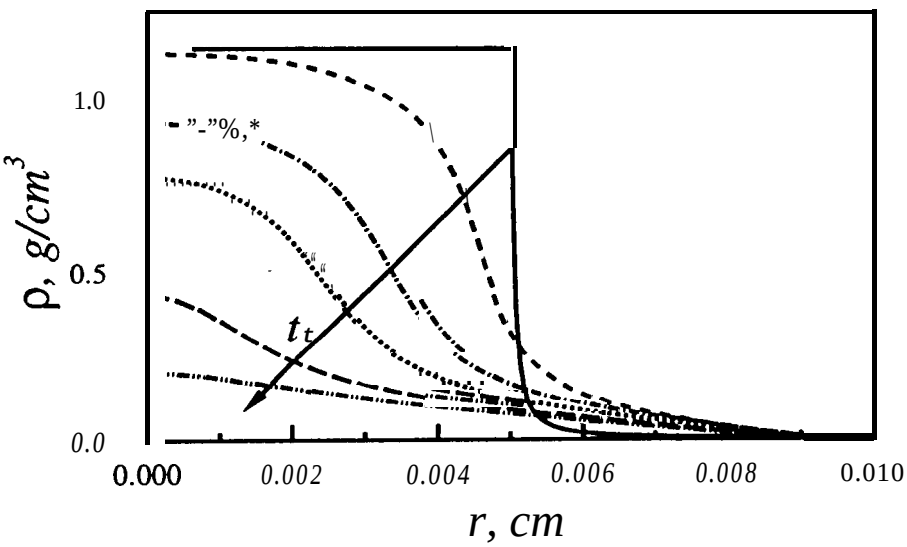

杉 1c

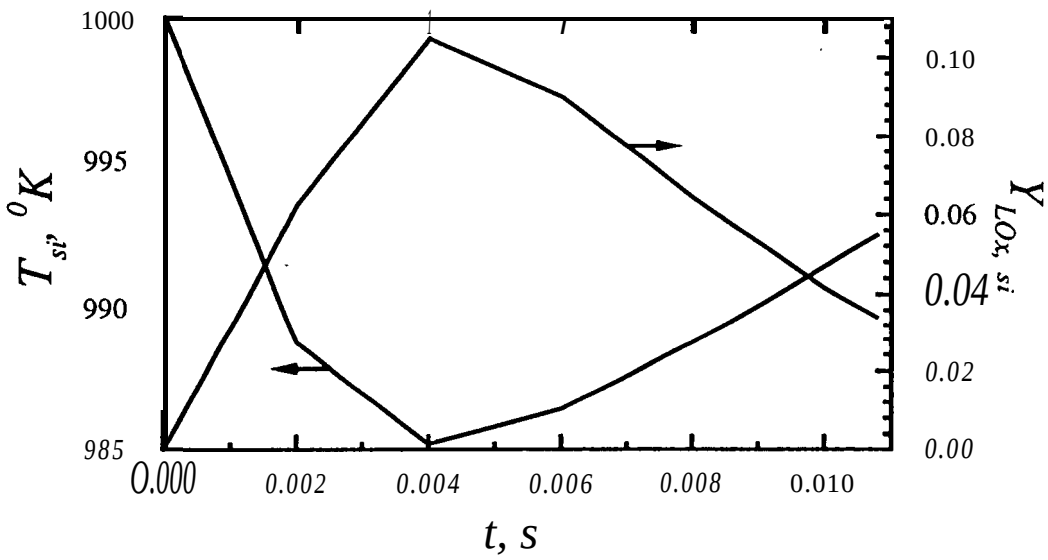
1000
995
990
985
T_{si}, ^0K
0.10
0.08
0.06
0.04
0.02
0.00
$Y_{Ox,si}$
0.000
0.002
0.004
0.006
0.008
0.010
t, s

Fig 2a

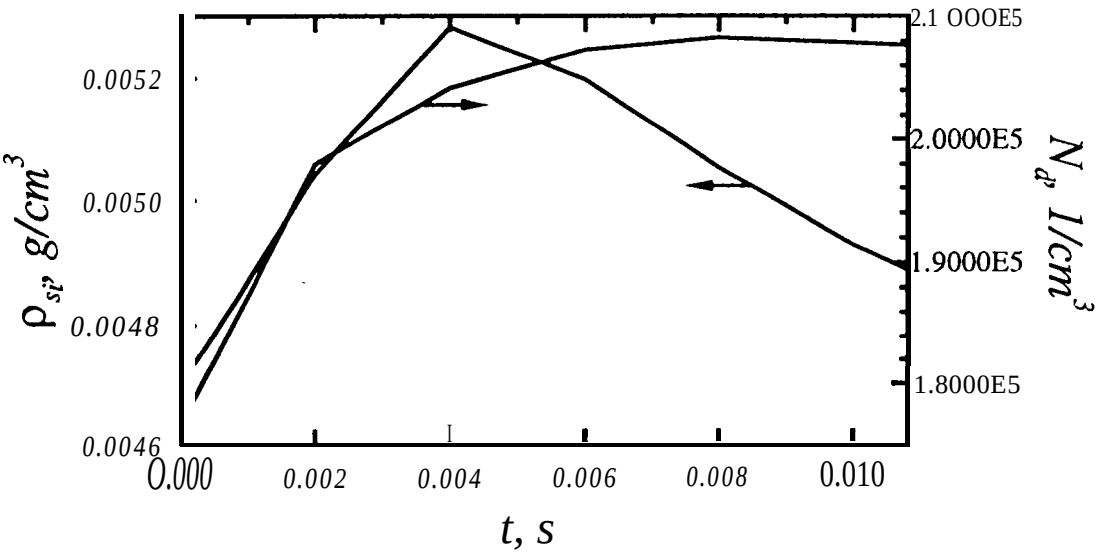
2.1 OOOE5
2.0000E5
1.9000E5
1.8000E5
0.0052
0.0050
0.0048
0.0046
0.000
0.002
0.004
0.006
0.008
0.010
t, s
ρ_{si}, g/cm^3
N_d, 1/cm^3

fig 2b

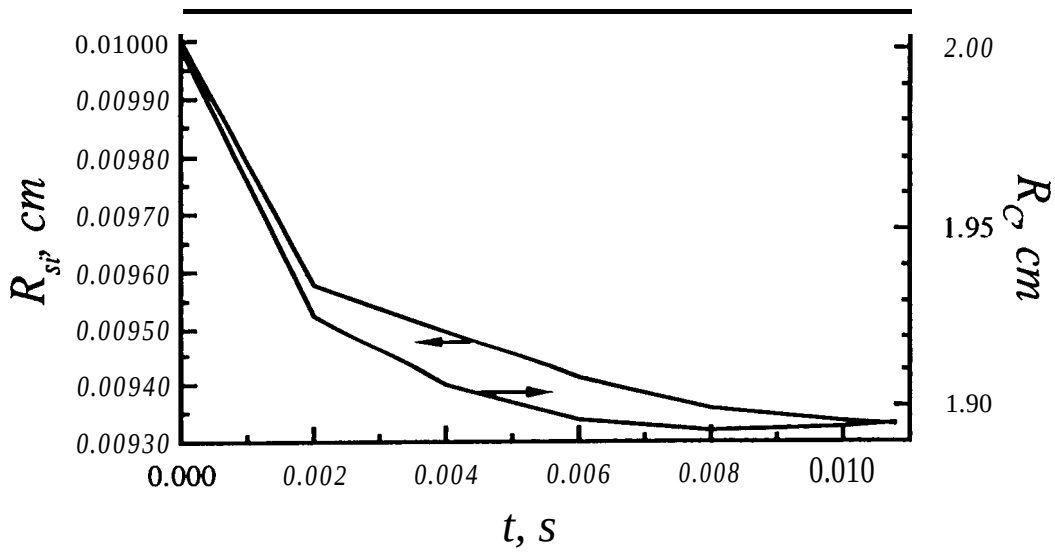
0.01000
0.00990
0.00980
0.00970
0.00960
0.00950
0.00940
0.00930
R_{si}, cm
2.00
1.95
1.90
R_C cm
0.000
0.002
0.004
0.006
0.008
0.010
t, s

Fig 2c

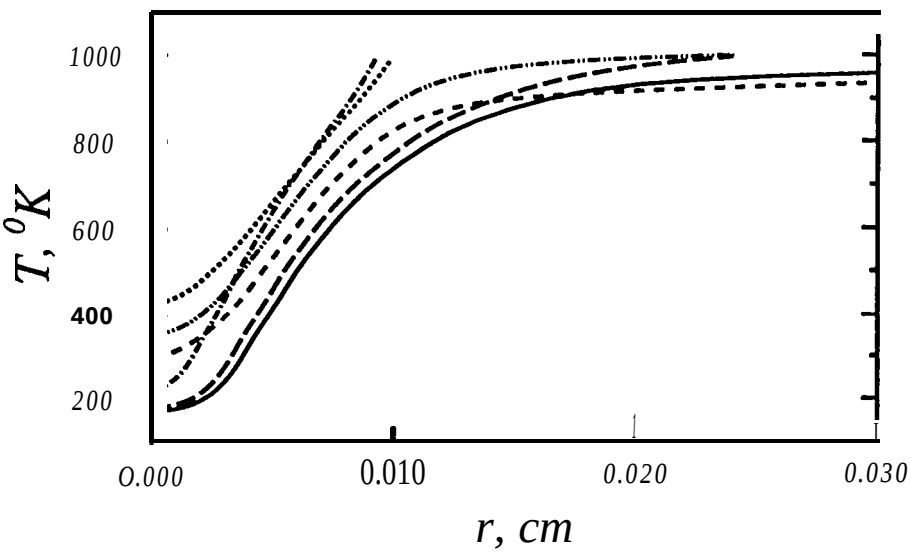

fig 3a

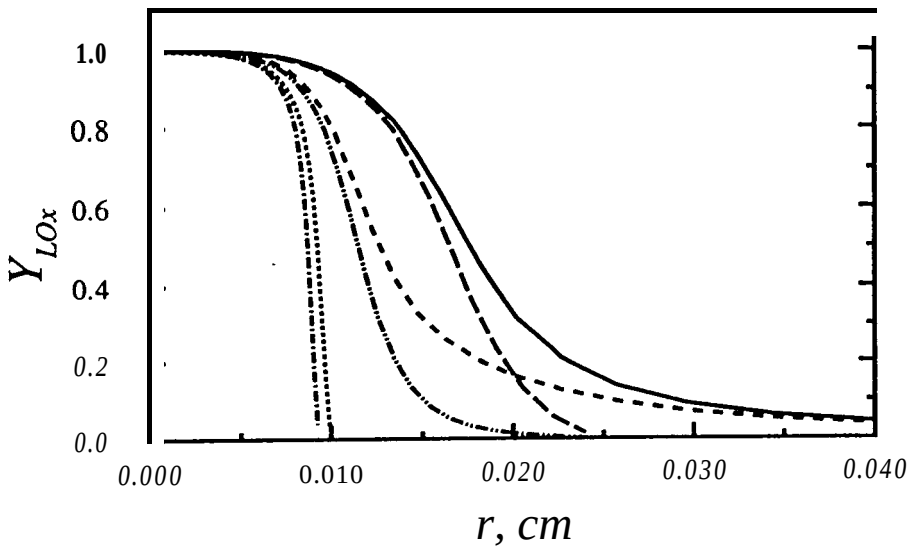

Fig 36

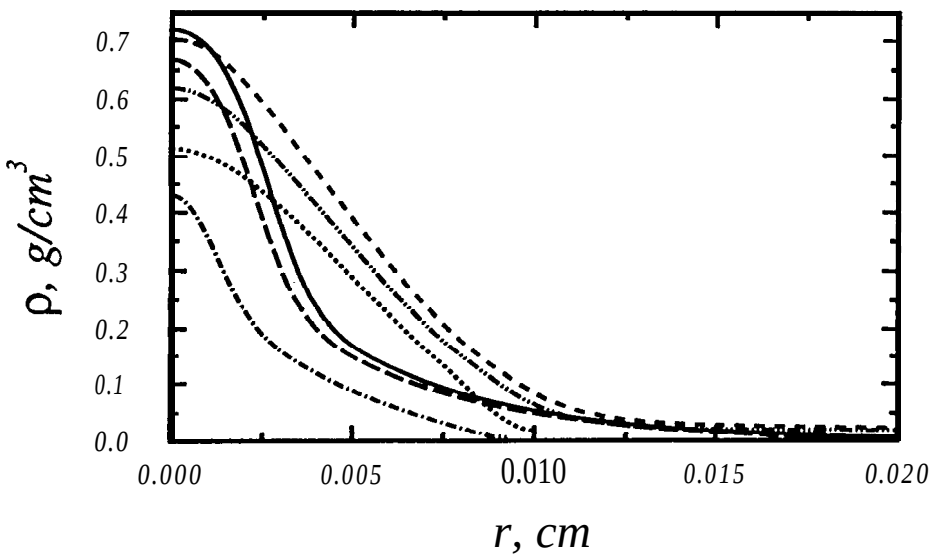

Fig 3c

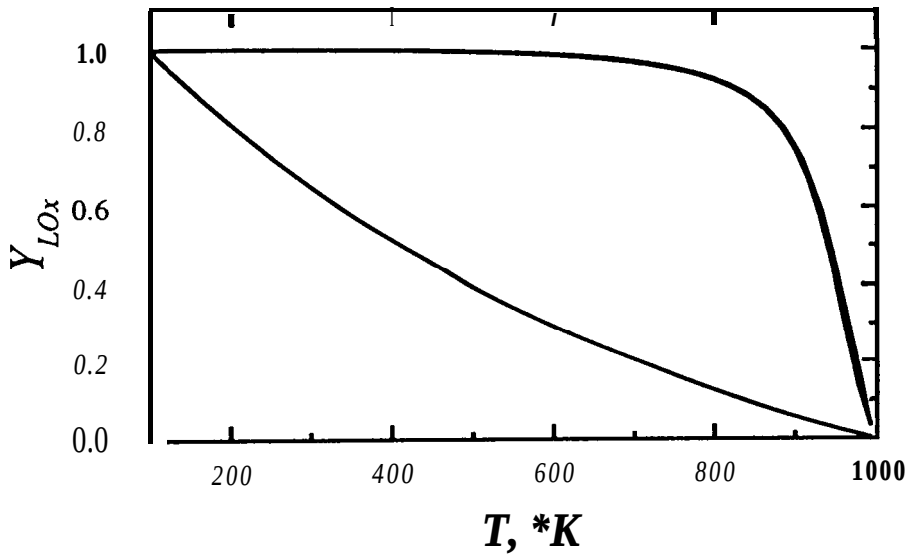

Fig 4

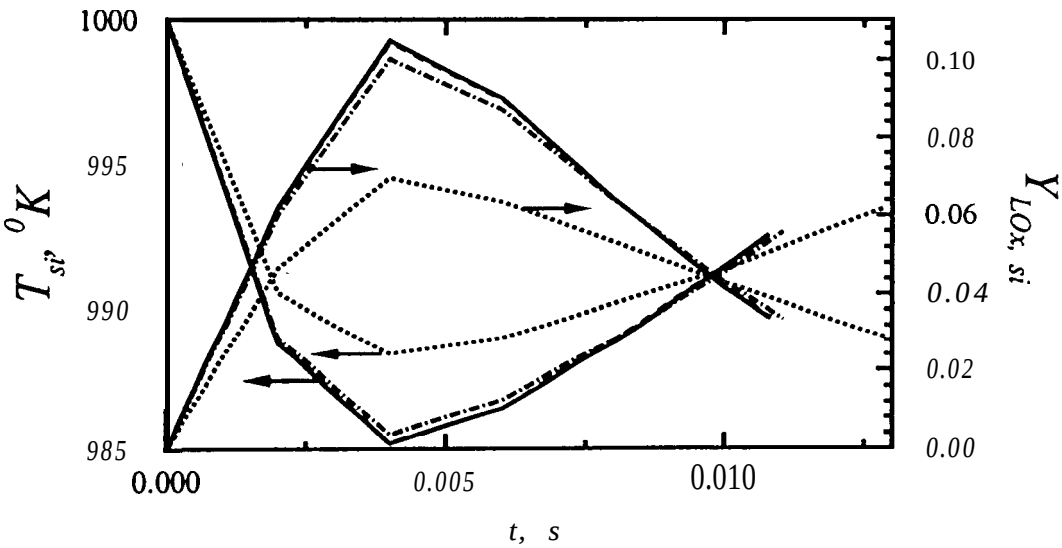
1000
995
990
985
0.000
0.005
0.010
t, s
T_{si}, ^0K
$Y_{Ox,\,si}$
0.10
0.08
0.06
0.04
0.02
0.00

Fig 3a

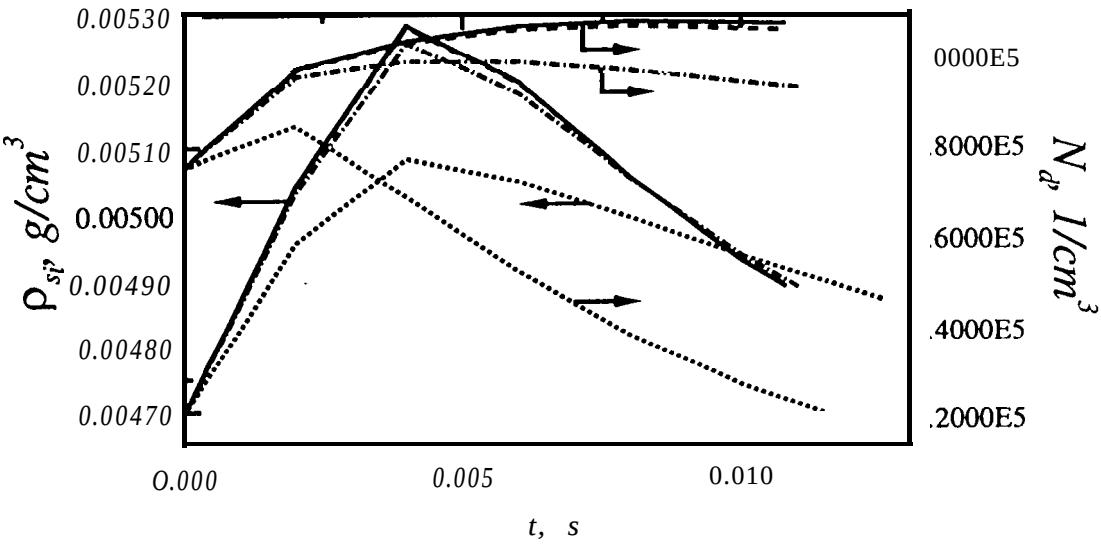
0.00530
0.00520
0.00510
0.00500
0.00490
0.00480
0.00470
ρ_{st}, g/cm^3
0000E5
.8000E5
.6000E5
.4000E5
.2000E5
N_d, 1/cm^3
0.000
0.005
0.010
t, s

Fig 5b.

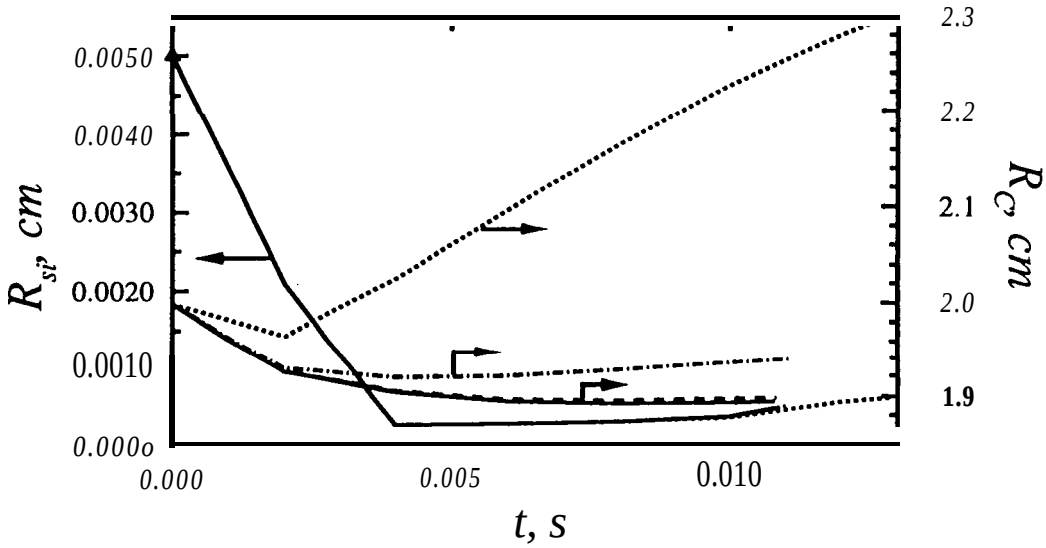
0.0050
0.0040
0.0030
0.0020
0.0010
0.000o
R_{sl}, cm
0.000
0.005
0.010
t, s
2.3
2.2
2.1
2.0
1.9
R_c cm

fig 5c.

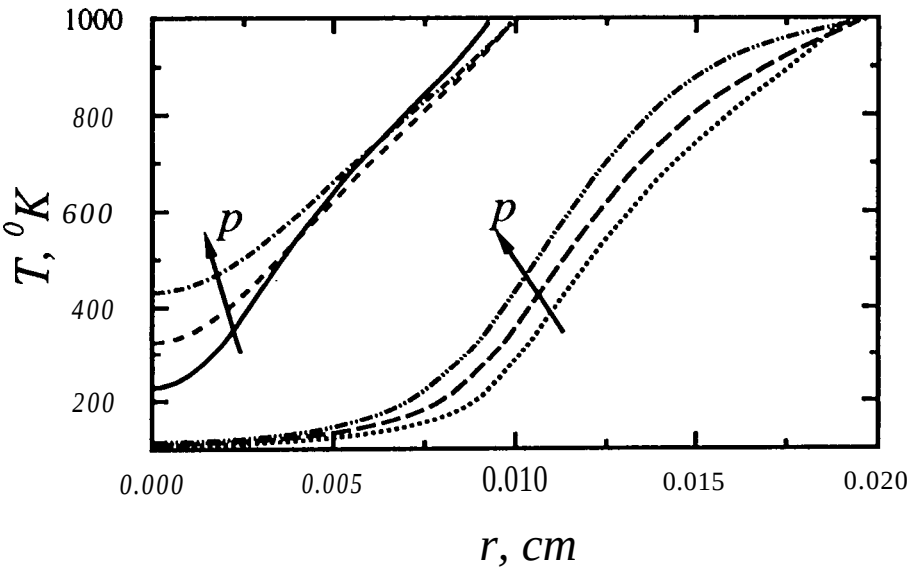

fig 6a

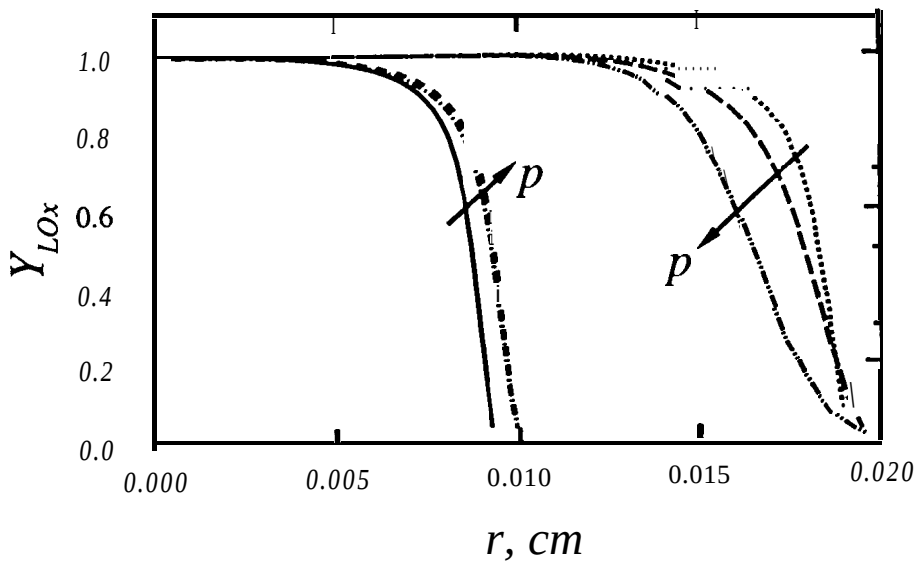

Fig 66

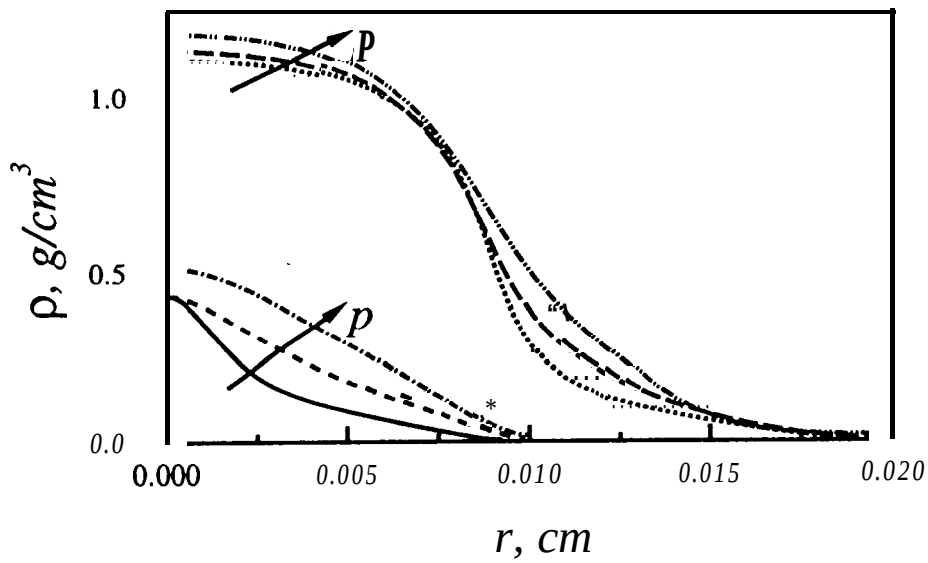

fig 6c

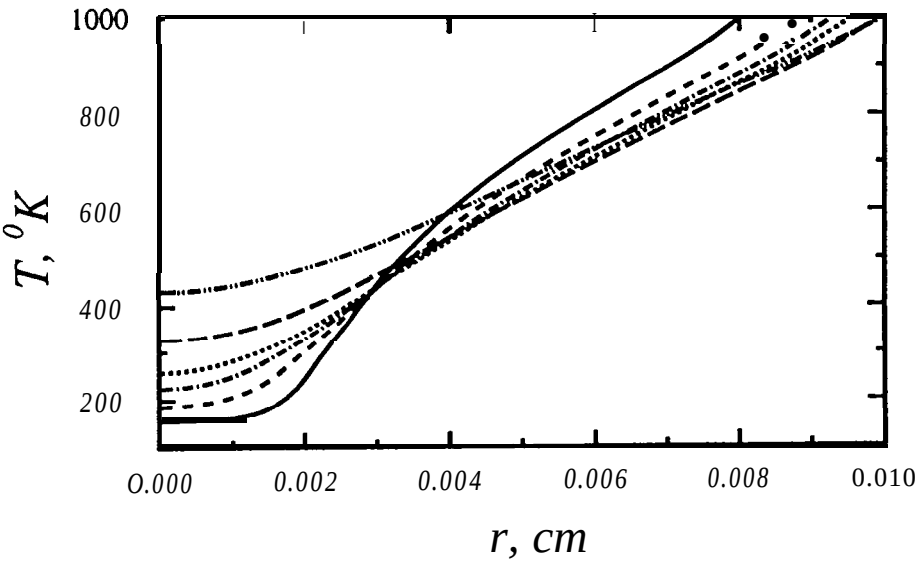

Fig 7a

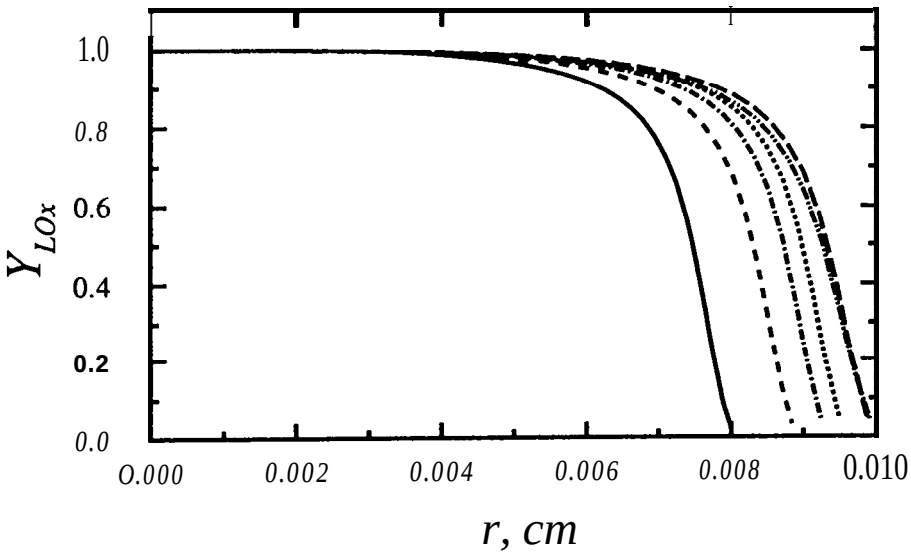

Fig 76

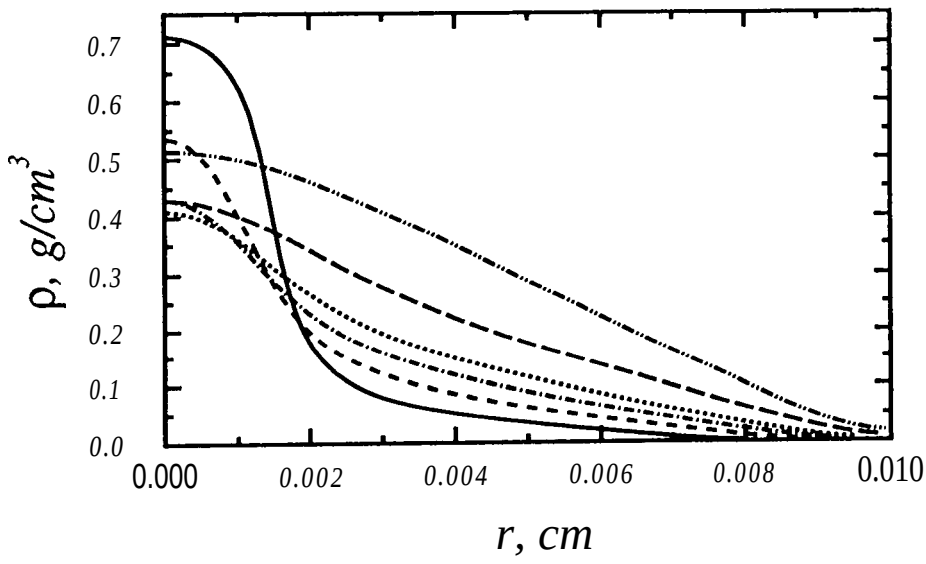

fig 7c